Superionic phases in the $(PbF_2)_{1-x}$-$(MF)_x$, M = K, Rb and Cs, systems

1999 J. Phys.: Condens. Matter 11 5257

(http://iopscience.iop.org/0953-8984/11/27/303)

J. Phys.: Condens. Matter **11** (1999) 5257–5272. Printed in the UK PII: S0953-8984(99)02288-2

Superionic phases in the $(PbF_2)_{1-x}$–$(MF)_x$, M = K, Rb and Cs, systems

S Hull and P Berastegui

The ISIS Facility, Rutherford Appleton Laboratory, Chilton, Didcot, Oxfordshire OX11 0QX, UK

Received 3 March 1999

Abstract. The ionic conductivity and crystal structure of PbF_2 doped with high concentrations of KF, RbF and CsF have been investigated at elevated temperatures using complex-impedance spectroscopy and powder neutron diffraction. In the case of $(PbF_2)_{1-x}$–$(KF)_x$, a high-temperature superionic phase with a body-centred-cubic cation sublattice is observed for $0.333 \leqslant x \lesssim 0.68$, in which the anions predominantly occupy the tetrahedral interstices. The corresponding phase in the $(PbF_2)_{1-x}(RbF)_x$ system is observed for $0.333 \leqslant x \leqslant 0.500$, though there is a gradual tendency towards cation ordering over the $0, 0, 0$ and $1/2, 1/2, 1/2$ sites as x increases. This process is accompanied by a change in the preferred anion sites in favour of a subset of the octahedral cavities, such that the mean structure tends towards a partially ordered perovskite-type arrangement. In the $(PbF_2)_{1-x}$–$(CsF)_x$ system only a single phase at a composition $x = 0.500$ is observed. This phase adopts a fully ordered perovskite structure and shows no evidence of superionic behaviour up to its melting point. The structural behaviour of the three $(PbF_2)_{1-x}(MF)_x$ systems with $M = K^+$, Rb^+ and Cs^+ is discussed in relation to the changes in the measured ionic conductivity with temperature and dopant concentration. The implications of these results for the wider question of possible superionic behaviour within halide perovskites is also discussed.

1. Introduction

Superionic conductors are materials which exhibit exceptionally high values of ionic conductivity whilst in the solid state. This behaviour usually only occurs at elevated temperatures, with values of the ionic conductivity ($\sigma \sim 0.1$–$1\ \Omega^{-1}\ cm^{-1}$) comparable to those for the liquid state above the melting point T_m. There are many examples of superionic compounds, including cation-mobile (e.g. Ag^+, Cu^+ and Li^+) and anion-mobile (e.g. O^{2-} and F^-) types [1]. Some of the highest values of σ are observed in the fluorine-ion conductors and it is possible to categorize the many known F^- superionic compounds on the basis of their crystal structure, as follows.

(a) Compounds such as β-PbF_2, CaF_2 and BaF_2 adopt the cubic fluorite crystal structure (space group $Fm\bar{3}m$) and are characterized by a rapid, though continuous, increase in σ (a type II superionic transition in the notation of Boyce and Huberman [2]). The gradual transition to the highly conducting state occurs at a temperature T_c of order $0.8T_m$. This process is characterized by an increasing concentration of short-lived, thermally activated anion Frenkel defects within the fluorite lattice [3]. β-PbF_2 has been widely studied because it has the lowest value of T_c in both absolute ($T_c = 710$ K) and relative ($T_c/T_m \sim 0.65$) terms [4]. It is also possible to enhance the ionic conductivity below T_c using chemical doping (e.g. with K^+ [5, 6] or Y^{3+} [7]) to introduce extrinsic defects (F^- vacancies and F^- interstitials, respectively).

0953-8984/99/275257+16$30.00

(b) There have been numerous, though often conflicting, investigations of possible superionic behaviour within fluoride compounds with the cubic perovskite crystal structure (space group $Pm\bar{3}m$). Whilst $KMgF_3$ and $KMnF_3$ are generally considered to be 'normal' conductors up to their melting points [8–10], there has been experimental evidence for a gradual increase in thermally induced F^- disorder within $KCaF_3$ [8, 10–12], $KZnF_3$ [13] and $NaMgF_3$ [14, 15]. However, the ionic conductivity measurements reported for the latter have been questioned and the high values of σ have been attributed to surface electronic conduction [9]. Furthermore, powder neutron diffraction studies of $NaMgF_3$ [16] and $KZnF_3$ [17] show increasingly anisotropic anion thermal vibrations at elevated temperatures but do not support the onset of the anion migration characteristic of superionic behaviour. In the wider sense, the possibility of superionic behaviour within perovskite-structured compounds is relevant to the field of earth sciences because the oxide perovskite (Mg, Fe)SiO_3 is the dominant constituent of the lower mantle and accounts for ∼70% of the earth by mass. The presence of extensive O^{2-} disorder has important consequences for the dynamic behaviour of the earth's interior and has implications for many geological problems, including changes in the earth's magnetic field with time (see [18–21]). However, perovskite-structured (Mg, Fe)SiO_3 is only thermodynamically stable at $p \gtrsim 25$ GPa and $T \gtrsim 1500$ K [22] and the halide compounds discussed above are ideal structural analogues which can be studied in more experimentally accessible temperature and pressure ranges.

(c) In a recent paper [23] we reported complex-impedance spectroscopy and neutron diffraction studies of a new structural class of fluorine-ion conductor formed by doping PbF_2 with 33 mol% KF. At a temperature of 520(5) K, the compound undergoes an abrupt (type I [2]) superionic transition with σ increasing by a factor ∼50×. The structure of the superionic phase comprises a b.c.c. cation sublattice formed by randomly arranged Pb^{2+} and K^+. The anions are extremely disordered, being distributed over the tetrahedral and, to a lesser extent, the octahedral interstices formed by the cation sublattice. As such, this phase can be considered to be 'anti-α-AgI' structured. However, it forms an interesting comparison with the situation observed in the superionic phase of AgI [24, 25] because it is the larger ionic species (F^-) that is mobile, rather than the smaller one (Ag^+). The possibility of investigating the effects of ionic size on the conduction mechanism has motivated further studies of fluorine-ion superionic compounds of this structure type, which are reported in this paper.

2. Experimental procedure

2.1. Sample preparation

Polycrystalline samples with composition $(PbF_2)_{1-x}$–$(MF)_x$, where M = K, Rb and Cs, were prepared by mixing stoichiometric amounts of the fluorides in a nitrogen filled dry box. Reactants had previously been dried overnight at 425 K in a vacuum oven. The samples were pelletized and then dried at 475 K for 2 h to remove any traces of moisture before sintering at 700 K for 15 h in a gold tube under a dynamic vacuum.

2.2. Ionic conductivity measurements

Two-terminal measurements of the ionic conductivity were performed using pelleted samples of ∼6 mm diameter and ∼6 mm length. These were held between two spring-loaded platinum discs inside a boron nitride cell which is inserted into the hot zone of a horizontal tube furnace.

Details of this device can be obtained elsewhere [26]. Complex-impedance measurements were performed approximately every three minutes whilst the furnace temperature was ramped up then down at 60 K h^{-1}. The maximum temperature used was ∼700 K. A Solartron S1260 Frequency Response Analyser determined the conventional Z–Z' Bode plot over the frequency range from 0.1 Hz to 10 MHz. The real component of the sample impedance Z_S was determined using the program IMMFIT [26]. All measurements were performed under a dynamic vacuum of $\sim 10^{-2}$ Pa and temperature monitoring achieved using chromel/alumel thermocouples located ∼2 mm from the sample pellet.

2.3. Neutron diffraction measurements

The diffraction experiments were performed on the Polaris powder diffractometer at the ISIS facility, UK [27], with the KF- and RbF-doped samples encapsulated inside thin-walled vanadium cans of ∼11 mm diameter and ∼40 mm height. The CsF-doped material is extremely reactive at elevated temperatures and was sealed under vacuum inside an ∼7 mm diameter silica ampoule of wall thickness ∼0.5 mm. High-temperature measurements used a special furnace designed for neutron diffraction constructed using a vanadium foil resistive heating element and heat shields. Diffraction data were predominantly collected using the backscattering detector bank which covers the scattering angles $135^\circ < \pm 2\theta < 160^\circ$ and provides data over the d-spacing range $0.5 < d$ (Å) < 3.2 with an essentially constant resolution of $\Delta d/d \sim 5 \times 10^{-3}$. Typical counting times were ∼2 h at each temperature. Rietveld profile refinements of the normalized diffraction data were performed using the program TF12LS [28], which is based on the Cambridge Crystallographic Subroutine Library [29]. The usual χ^2-statistic was used to assess the relative merits of different structural models applied to the data, where χ^2 is the ratio of the square of the standard weighted profile R-factor, R_w, to the square of the expected R-factor, R_{exp} [30].

3. Results

3.1. $(PbF_2)_{1-x}$–$(KF)_x$

Our previous paper described the ionic conductivity and structural behaviour of PbF_2 doped with KF over the range $0 \leqslant x \leqslant 0.333$ [23]. At the highest concentration a superionic phase was observed at temperatures in excess of 520(5) K, with the ionic conductivity σ increasing by a factor ∼50× at the transition and saturating at a value close to ∼0.4 Ω^{-1} cm^{-1}. To investigate the stability range of this superionic phase as a function of increasing KF content, the ionic conductivity of samples doped with $x = 0.333$, 0.400, 0.450, 0.500, 0.550, 0.625 and 0.700 was measured. Selected plots are illustrated in figure 1. The superionic transition is observed for all compositions except that with $x = 0.700$, though the discontinuity in σ decreases with x. In addition, the transition temperature T_c increases steadily with x, as listed in table 1. The results for the ionic conductivity at a representative temperature of 675(2) K within the superionic phase are illustrated in figure 2(a).

The investigation of the structural behaviour of the superionic phase of $(PbF_2)_{1-x}$–$(KF)_x$ with KF content x used neutron diffraction data collected from samples with $x = 0.333$, 0.400, 0.500, 0.600 and 0.700. Data for the $x = 0.333$ sample were presented in our previous paper [23], indicating that a transition occurs at $T \sim 520(5)$ K which is coincident with the abrupt jump in the ionic conductivity σ (see figure 1). The high-temperature superionic phase was determined to be cubic, with $a = 4.6655(1)$ Å and space group $Im\bar{3}m$. The Pb^{2+} and K^+ cations are randomly distributed over the two sites at $0, 0, 0$ and $1/2, 1/2, 1/2$ and the

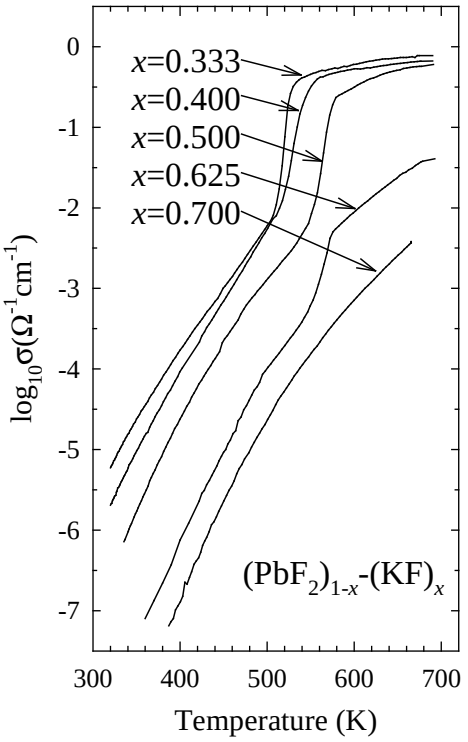

Figure 1. Variation of the ionic conductivity $\log_{10}\sigma$ with temperature for $(PbF_2)_{1-x}$–$(KF)_x$ samples with $x = 0.333$, 0.400, 0.500, 0.625 and 0.700.

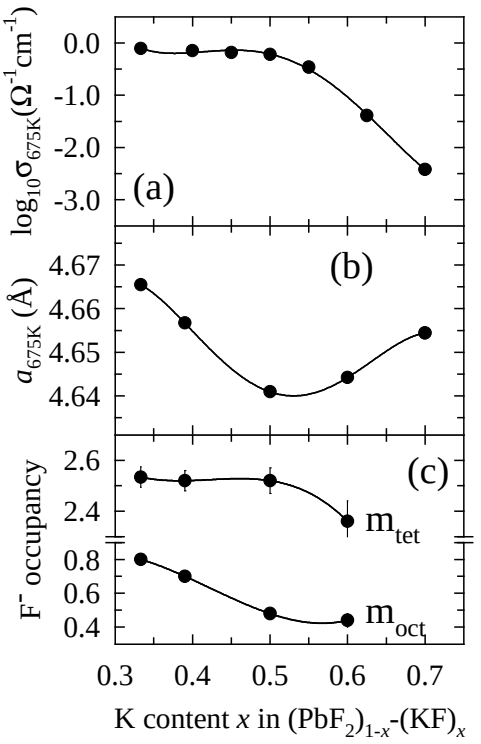

Figure 2. Variation of (a) the ionic conductivity $\log_{10}\sigma$, (b) the cubic lattice parameter a and (c) the F^- occupancy of the tetrahedral (m_{tet}) and octahedral (m_{oct}) sites versus KF content x in $(PbF_2)_{1-x}$–$(KF)_x$. The data all correspond to a temperature of 675(2) K.

F^- are disordered over the tetrahedral and, to a lesser extent, the octahedral interstices (see figure 3(a)). Inspection of the diffraction data collected from the $(PbF_2)_{1-x}$–$(KF)_x$ samples with $x > 0.333$ at high temperature showed that the diffraction pattern comprised entirely that expected from a body-centred-cubic structure of this type. However, at $x = 0.700$ additional weak reflections are observed in addition to those expected for the b.c.c. superionic phase. It seems likely, therefore, that the superionic phase is stable up to $x \sim 0.68$ and that the additional peaks are due to the presence of a small amount of a phase with higher K^+ content. A possible candidate is the phase of composition PbK_4F_6 observed previously [31, 32].

The analysis of the neutron diffraction data collected within the high-temperature superionic phase of $(PbF_2)_{1-x}$–$(KF)_x$ follows that adopted previously for the $x = 0.333$ case [23]. However, a larger set of structural models are used to fit the experimental data, to include the possibility of partial or complete ordering of the cation and anion sublattices. Clearly, the absence of any measurable intensity at any of the $h + k + l \neq 2n$ Bragg positions forbidden in $Im\bar{3}m$ symmetry provides no evidence for such long-range order. However, this more general approach allows us to use the same set of structural models to subsequently analyse the diffraction data for the $(PbF_2)_{1-x}$–$(RbF)_x$ and $(PbF_2)_{1-x}$–$(CsF)_x$ systems in subsections 3.2 and 3.3, respectively. The models are divided into four main classes, labelled I to IV.

The simplest approach is the 'model-independent' fit (labelled I) in which the neutron diffraction data are fitted by varying the intensities of each of the Bragg intensities, plus the

Table 1. Summary of the samples investigated in the course of this work. The dopant content x in $(PbF_2)_{1-x}$–$(MF)_x$ is given. The quantity y gives the deviation from the idealized perovskite stoichiometry in $MPbF_{3+y}$ and T_c is the superionic transition temperature.

Dopant M	x in $(PbF_2)_{1-x}$–$(MF)_x$	y in $M_{1+y}Pb_{1-y}F_{3-y}$	T_c (K)
K	0.333	−0.333	520(5)
	0.400	−0.200	543(6)
	0.450	−0.100	560(6)
	0.500	0.000	568(7)
	0.550	0.100	570(7)
	0.625	0.250	578(8)
	0.700	0.400	588(12)
Rb	0.333	−0.333	619(6)
	0.350	−0.300	617(6)
	0.375	−0.250	612(7)
	0.400	−0.200	597(8)
	0.425	−0.150	576(10)
	0.475	−0.050	575(10)
	0.500	0.000	∼ 350
Cs	0.500	0.000	—

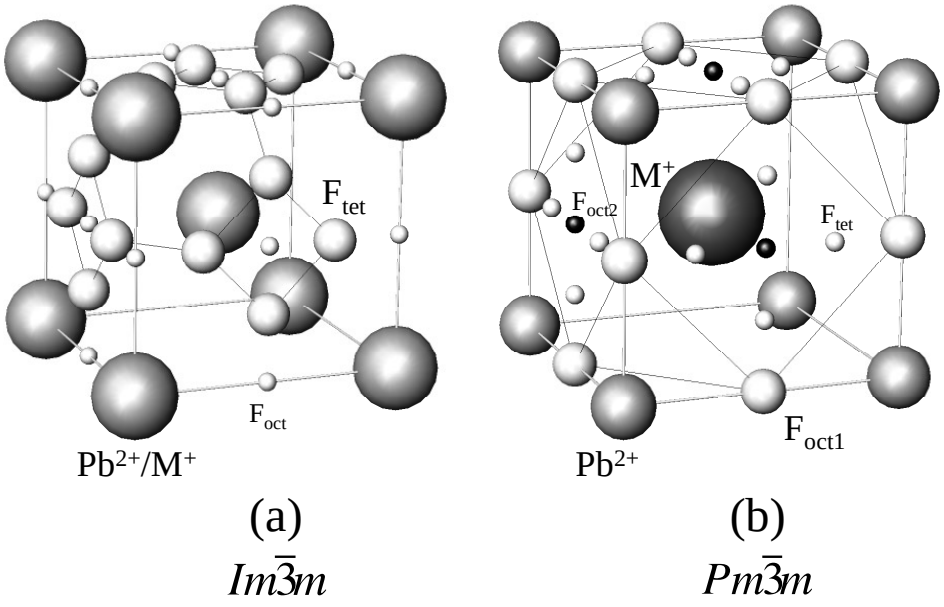

Figure 3. (a) A schematic diagram of the structure of the anti-α-AgI type b.c.c. superionic phase of $(PbF_2)_{1-x}$–$(MF)_x$ with $x = 0.333$. The cations Pb^{2+} and M^+ are distributed over the $0, 0, 0$ and $1/2, 1/2, 1/2$ positions. The preferred F^- locations within the tetrahedral (F_{tet}) and octahedral (F_{oct}) voids are shown. (b) illustrates a perovskite-structured phase of composition $MPbF_3$, with the two cation species ordered such that the M^+ occupy the $1/2, 1/2, 1/2$ positions (A sites) and Pb^{2+} the $0, 0, 0$ positions (B sites). The anions are located at the sites labelled F_{oct1}, with the tetrahedral F_{tet} positions empty. In the ideal case, the alternative set of octahedral sites labelled F_{oct2} are also empty.

cubic lattice parameter a, a parameter describing the Gaussian width of the Bragg peaks and coefficients describing a polynomial representation of the background scattering component. This approach assumes no structural information concerning the high-temperature phase other than its space group, which is taken to be $Pm\bar{3}m$ so as not to assume *a priori* that the lattice is body centred (i.e. cation disordered). As a result, this model provides a 'best fit' to the experimental data and gives an indication of the value of the goodness-of-fit parameter χ^2 expected during subsequent fits which impose structural constraints during the least-squares procedure. The values obtained are listed in table 2.

Table 2. Summary of the goodness-of-fit parameter χ^2 obtained by fitting the neutron data for the $(PbF_2)_{1-x}$–$(MF)_x$ systems using the structural models I to IV described in section 3.1. The best fit is shown by underlining. The symbol ○ indicates that the fit was unstable and failed to converge whilst × indicates a fit which is rejected because it gave non-physical values of the fitted parameters (usually temperature factors and/or site occupancies less than zero). Symbols such as →IIc indicate that the fit converged with values of certain site occupancies zero or equal (within error) such that the derived structure is equivalent to that described by a simpler model with fewer variable parameters.

		Structural model										
		None	Cations disordered			Cations partly ordered				Cations ordered		
Dopant		$Pm\bar{3}m$	$Im\bar{3}m$			$Pm\bar{3}m$				$Pm\bar{3}m$		
M^+	x	I	IIa	IIb	IIc	IIIa	IIIb	IIIc	IIId	IVa	IVb	IVc
K	0.333	0.98	5.87	4.57	<u>1.13</u>	—	○	3.30	×	—	—	—
	0.390	1.10	6.17	4.33	<u>1.17</u>	—	→IIa	3.27	→IIc	—	—	—
	0.500	1.07	7.17	4.01	<u>1.22</u>	7.56	○	4.03	○	10.71	8.22	8.13
	0.600	1.13	6.99	5.12	<u>1.25</u>	7.44	→IIa	3.18	○	—	—	—
Rb	0.333	1.17	6.01	4.22	1.32	—	1.67	1.39	<u>1.20</u>	—	—	—
	0.350	1.09	5.13	3.80	1.37	—	1.88	<u>1.24</u>	1.22	—	—	—
	0.375	0.99	6.22	4.71	1.50	—	1.80	<u>1.13</u>	→IIIc	—	—	—
	0.400	1.10	6.12	5.06	1.62	—	1.73	<u>1.22</u>	→IIIc	—	—	—
	0.425	1.20	7.71	6.11	2.30	—	1.62	<u>1.27</u>	→IIIc	—	—	—
	0.450	1.11	7.02	5.82	2.12	—	1.77	<u>1.19</u>	○	—	—	—
	0.500	1.24	6.81	5.31	2.74	3.20	1.93	→IIc	→IIc	3.71	2.02	<u>1.30</u>
Cs	0.500	1.04	6.12	8.07	○	→IIa	→IIa	→IIa	○	1.18	→IVa	→IVa

Model II assumes there is no long-range order of either cation sublattice and the space group is then $Im\bar{3}m$. With reference to figure 3(a), the Pb^{2+} and K^+ are distributed randomly over the 2(a) positions at $0, 0, 0$ and $1/2, 1/2, 1/2$. The resultant body-centred-cubic cation sublattice provides six octahedral cavities at the 6(b) positions at $0, 1/2, 1/2$ etc and twelve tetrahedral interstices located at the 12(d) sites at $1/4, 0, 1/2$ etc. These potential anion positions are labelled F_{tet} and F_{oct}, respectively. Models IIa and IIb constrain the anions to randomly occupy the F_{tet} and F_{oct} sites, respectively, whilst model IIc allows the occupancies of the two sites (m_{tet} and m_{oct}) to vary independently. However, in all of the fits the total anion content within the unit cell is constrained to be equal to the value determined by the dopant concentration x (i.e. $m_{tet} + m_{oct} = 2(2 - x)$). Model IIc corresponds to the structural model which has been found previously to best fit the diffraction data for the superionic phase of the $x = 0.333$ sample [23].

Model III considers the possibility of (at least partial) ordering of the two cation species over the two sites in the unit cell. This corresponds to space group $Pm\bar{3}m$, in which the symmetry-independent sites are now 1(a) at $0, 0, 0$ and 1(b) at $1/2, 1/2, 1/2$. The occupancies

of these two sites are thus allowed to vary, with the constraints that both are always fully filled and that the overall content of Pb^{2+} and K^+ equals the chemical composition given by x. The reduction in symmetry from $Im\bar{3}m$ to $Pm\bar{3}m$ does not change the multiplicity of the F_{tet} positions, which become the 12(h) sites at $x_{F\,tet}$, $1/2, 0$ etc with the value of the variable position parameter $x_{F\,tet} = 1/4$. However, the six octahedral sites form two symmetry-independent threefold sets in 3(d) positions at $1/2, 0, 0$ etc and in 3(c) positions at $0, 1/2, 1/2$ etc. These are labelled F_{oct1} and F_{oct2}, respectively (see figure 3(b)). In principle, the number of structural models is increased, though the number of *different* configurations is reduced by noting that the structure is topologically identical if we simultaneously swap the occupancies of the both the 1(a) and 1(b) sites and the 3(d) and 3(c) positions. Thus, allowing the cation distribution to vary completely over the 1(a) and 1(b) sites does not require us to separately test models which use F_{oct1} and F_{oct2} positions. Model IIIa places all the anions on the F_{oct1} positions and model IIIb distributes the anions over the F_{oct1} and F_{oct2} positions. In the former, the number of available sites for anions requires $m_{oct1} \leqslant 3.0$ and this model is thus only valid for samples with $x \geqslant 0.500$. Models IIIc and IIId are extensions of models IIIa and IIIb respectively, allowing a fraction of the anions to additionally occupy the F_{tet} positions.

Model IV can be considered to be a special case of the model III, in which the cations are constrained to be fully ordered over the 1(a) and 1(b) sites of space group $Pm\bar{3}m$. As such, it is only appropriate for those samples with $x = 0.500$. We place the smaller cation (Pb^{2+}) at the 1(a) site at $0, 0, 0$ and the larger (K^+) in the 1(b) position at $1/2, 1/2, 1/2$. As a result, the F_{oct1} interstices are larger than the F_{oct2} ones (see below) and in model IVa only the former are included. These anion sites are fully occupied and the ionic arrangement corresponds to the ordered perovskite structure. In the usual notation for perovskite-structured compounds of composition ABX_3, the larger A cation occupies the 1(b) site, the smaller B cation resides in the 1(a) position and the X anions are at 3(d) sites. In models IVb and IVc the possibility of a degree of disorder within the perovskite structure is considered, by allowing a variable fraction of the anions to also occupy F_{oct2} and F_{tet} sites, respectively.

The values of χ^2 obtained by fitting the experimental data for the high-temperature superionic phase of $(PbF_2)_{1-x}$–$(KF)_x$ using models I to IV are listed in table 2. The data for the $x = 0.700$ sample were not considered in any detail owing to the presence of the second phase of possible composition PbK_4F_6 and unknown structure. In all other cases, model IIc is found to provide the best fit to the experimental data, in accord with the results for the $x = 0.333$ case presented previously [23]. Model III produced poorer or unstable fits to the data, or tended to converge with parameter values essentially the same as those provided by model IIc. There is then no indication of even partial ordering of either cations or anions, as might be expected intuitively given the apparent body-centred nature of the structure implied by the diffraction data. Similarly, attempts to fit the data for the $x = 0.500$ sample with the fully ordered model IV proved unsuccessful. The results of the fits are given in table 2 and the values of lattice parameter a and the site occupancies m_{tet} and m_{oct} are illustrated in figures 2(b) and 2(c), respectively.

3.2. $(PbF_2)_{1-x}$–$(RbF)_x$

The impedance spectroscopy and neutron diffraction measurements of the $(PbF_2)_{1-x}$–$(RbF)_x$ system used samples with $x = 0.333$, 0.350, 0.375, 0.400, 0.425, 0.475 and 0.500. Representative data for the ionic conductivity are illustrated in figure 4. The data for the $x = 0.333$ sample resemble that for its K^+-doped counterpart, though the superionic transition occurs at a somewhat higher temperature of $T_c = 619(6)$ K. With increasing dopant concentration x, the transition occurs at lower temperatures and is somewhat broader. In

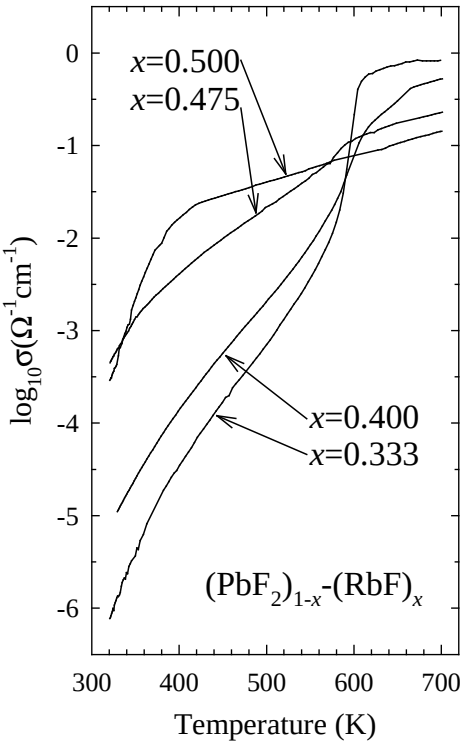

Figure 4. Variation of the ionic conductivity $\log_{10}\sigma$ with temperature for $(PbF_2)_{1-x}$–$(RbF)_x$ samples with $x = 0.333$, 0.400, 0.475 and 0.500.

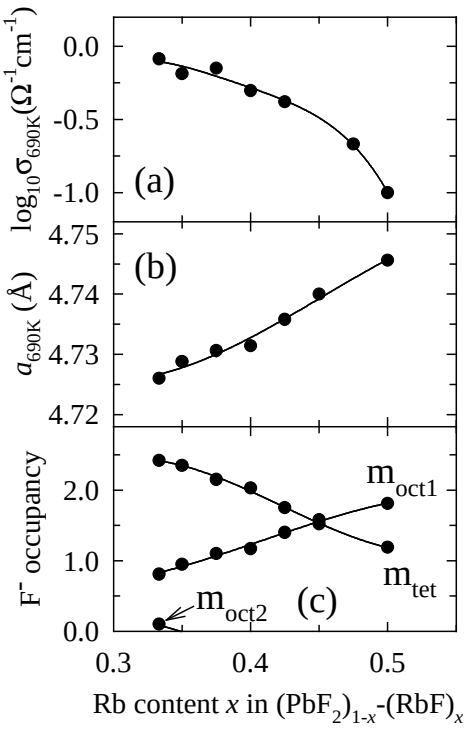

Figure 5. Variation of (a) the ionic conductivity $\log_{10}\sigma$, (b) the cubic lattice parameter a and (c) the F^- occupancy of the tetrahedral (m_{tet}) and two octahedral (m_{oct1} and m_{oct2}) sites versus RbF content x in $(PbF_2)_{1-x}$–$(RbF)_x$. The data all correspond to a temperature of 690(2) K.

addition, the value of the ionic conductivity σ above the transition decreases with increasing x. These results are summarized in table 1 and figure 5(a). The sample with $x = 0.500$ behaves somewhat differently to the others, with no evidence of a superionic transition in the region $T \sim 550$–600 K. Instead, the sample has a relatively high ionic conductivity above ∼400 K.

A portion of the diffraction pattern collected for the $x = 0.333$ sample over the temperature range $295 < T$ (K) < 690 is illustrated in figure 6. The abrupt change in the diffraction pattern at $T \sim 620$ K is clearly visible, as the additional peaks observed at low temperature disappear. This change is obviously associated with the abrupt jump in σ (figure 4). Above the transition the diffraction pattern is very similar to that observed in the $(PbF_2)_{1-x}$–$(KF)_x$ case, with the ∼15 observed Bragg peaks indexed on a body-centred-cubic unit cell with $a \sim 4.7260(1)$ Å. However, inspection of the data collected for the samples with $x > 0.333$ illustrates a gradual appearance of additional weak reflections at the 'forbidden' positions with $h + k + l = 2n$. This behaviour is illustrated for the case of the 111 reflection in figure 7. This observation is indicative of the onset of ordering of either the cation or the anion sublattice (or both). This intuition is borne out by the results of fitting the data collected at 690 K (table 2) which show that the partially ordered model III provides the best fit to the data for samples with $0.333 \leqslant x \leqslant 0.500$. This is true even in the case of the $x = 0.333$ material where none of the additional Bragg peaks indicative of $Pm\bar{3}m$ are visible, though the improvement over model IIc is relatively small for the two lowest-x cases. The preference for a least partial

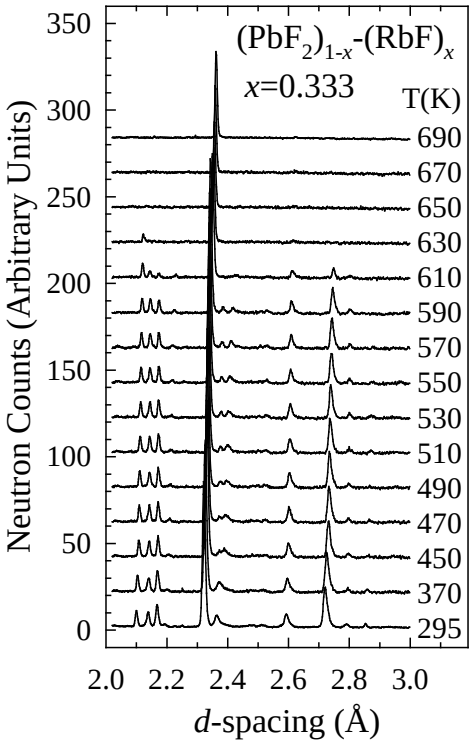

Figure 6. The evolution of the neutron diffraction pattern of the $(PbF_2)_{1-x}$–$(RbF)_x$ sample with $x = 0.333$ with temperature. The structural transition to the superionic b.c.c.-structured phase at $T \sim 620$ K is clearly visible.

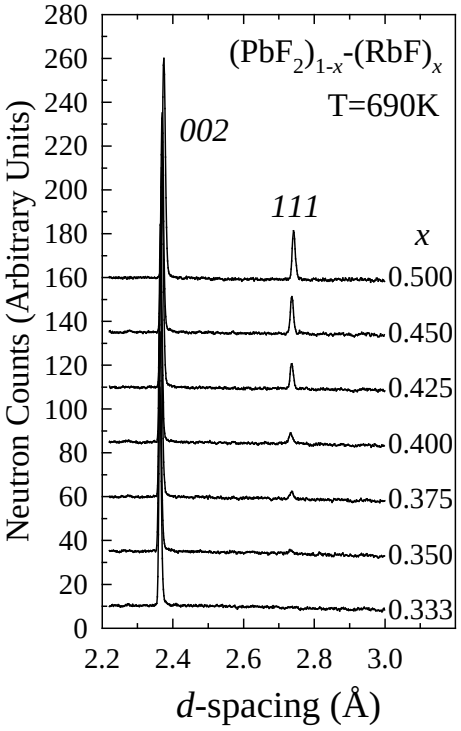

Figure 7. A portion of the diffraction pattern collected from the $(PbF_2)_{1-x}$–$(RbF)_x$ samples with $x = 0.333$, 0.350, 0.375, 0.400, 0.425, 0.450 and 0.500 at a temperature of 690(2) K. The gradual appearance of the 111 reflection which is forbidden in $Im\bar{3}m$ symmetry with increasing x is illustrated.

occupancy of the tetrahedral sites is clearly observed and, with the exception of the case of the $x = 0.333$ sample, model IIIc is favoured over model IIIb indicating a preference for occupancy of only one of the octahedral positions. The structural implications of these results (listed in table 3) will be discussed in section 4.

The evolution of the diffraction pattern for the $x = 0.500$ sample with temperature is shown in figure 8. Unfortunately, difficulties in controlling the temperature of the furnace at temperatures below ∼400 K prevented studies from being made for the crucial temperature range where the ionic conductivity changes rapidly (see figure 4). However, comparison of the data collected at 295 K and 400 K illustrates that a structural change has taken place, though the low-temperature material is characterized by both a broadening of the Bragg peaks characteristic of the high-temperature phase and the appearance of additional weak reflections that are also observed in the $x = 0.333$ sample at room temperature. This implies that the room temperature structure is related to that of the high-temperature superionic phase and that the latter might be stabilized at ambient temperature by, for example, the addition of further dopants or rapid quenching from high temperature. Further studies are planned to investigate this possibility. Analysis of the data collected at 690 K shows that it is best fitted using model IVc, in which the cations are fully ordered over the $0, 0, 0$ and $1/2, 1/2, 1/2$ sites and the anions are distributed over the F_{oct1} and F_{tet} positions. The results are summarized in table 3.

Table 3. The results of the fits to the neutron diffraction data for the $(PbF_2)_{1-x}$–$(MF)_x$ systems. The temperature factors (B) and site occupancies (m) are given for the best fit using the structural model listed in the second column (see section 3.1 for a description).

Dopant		'Best'	Cation B site at (0, 0, 0)		Cation A site at (1/2, 1/2, 1/2)	
M^+	x	model	B_B (Å^2)	Occupancies	B_A (Å^2)	Occupancies
K	0.330	IIc	6.3(2)	$m_{Pb} = 0.667$	$=B_B$	$m_{Pb} = 0.667$
				$m_K = 0.333$		$m_K = 0.333$
	0.390	IIc	6.5(2)	$m_{Pb} = 0.610$	$=B_B$	$m_{Pb} = 0.610$
				$m_K = 0.390$		$m_K = 0.390$
	0.500	IIc	7.0(3)	$m_{Pb} = 0.500$	$=B_B$	$m_{Pb} = 0.500$
				$m_K = 0.500$		$m_K = 0.500$
	0.600	IIc	6.4(2)	$m_{Pb} = 0.400$	$=B_B$	$m_{Pb} = 0.400$
				$m_K = 0.600$		$m_K = 0.600$
Rb	0.333	IIId	5.9(7)	$m_{Pb} = 0.87(7)$	5.3(6)	$m_{Pb} = 0.46(7)$
				$m_{Rb} = 0.13(7)$		$m_{Rb} = 0.54(7)$
	0.350	IIIc	5.6(3)	$m_{Pb} = 0.97(3)$	5.7(4)	$m_{Pb} = 0.33(3)$
				$m_{Rb} = 0.03(3)$		$m_{Rb} = 0.67(3)$
	0.375	IIIc	5.8(2)	$m_{Pb} = 0.98(3)$	5.9(3)	$m_{Pb} = 0.27(3)$
				$m_{Rb} = 0.02(3)$		$m_{Rb} = 0.73(3)$
	0.400	IIIc	5.4(1)	$m_{Pb} = 0.96(3)$	6.2(2)	$m_{Pb} = 0.24(3)$
				$m_{Rb} = 0.04(3)$		$m_{Rb} = 0.76(3)$
	0.425	IIIc	5.3(1)	$m_{Pb} = 1.02(2)$	6.6(2)	$m_{Pb} = 0.13(2)$
				$m_{Rb} = -0.02(2)$		$m_{Rb} = 0.87(2)$
	0.450	IIIc	5.2(1)	$m_{Pb} = 0.98(2)$	5.9(1)	$m_{Pb} = 0.12(2)$
				$m_{Rb} = 0.02(2)$		$m_{Rb} = 0.88(2)$
	0.500	IVc	5.2(1)	$m_{Pb} = 1.000$	7.0(2)	$m_{Pb} = 0.000$
				$m_{Rb} = 0.000$		$m_{Rb} = 1.000$
Cs	0.500	IVa	3.4(1)	$m_{Pb} = 1.000$	5.8(1)	$m_{Pb} = 0.000$
				$m_{Cs} = 1.000$		$m_{Cs} = 0.000$

Dopant		'Best'	F_{tet} tetrahedral site at (1/4, 0, 1/2) etc		F_{oct1} octahedral site at (0, 0, 1/2) etc		F_{oct2} octahedral site at (1/2, 1/2, 0) etc	
M^+	x	model	$B_{F\,tet}$ (Å^2)	$m_{F\,tet}$	$B_{F\,oct1}$ (Å^2)	$m_{F\,oct1}$	$B_{F\,oct2}$ (Å^2)	$m_{F\,oct2}$
K	0.330	IIc	10.4(3)	2.53(2)	8.7(6)	0.40(1)	$=B_{F\,oct1}$	$=m_{F\,oct1}$
	0.390	IIc	9.7(4)	2.52(2)	8.4(5)	0.35(1)	$=B_{F\,oct1}$	$=m_{F\,oct1}$
	0.500	IIc	10.0(4)	2.52(2)	9.2(5)	0.24(1)	$=B_{F\,oct1}$	$=m_{F\,oct1}$
	0.600	IIc	9.3(3)	2.36(4)	8.7(4)	0.22(2)	$=B_{F\,oct1}$	$=m_{F\,oct1}$
Rb	0.333	IIId	13.1(8)	2.42(7)	7.7(8)	0.81(7)	$=B_{F\,oct1}$	0.10(7)
	0.350	IIIc	14.3(7)	2.35(3)	7.6(6)	0.95(3)	—	0.000
	0.375	IIIc	13.5(6)	2.15(3)	8.1(5)	1.10(3)	—	0.000
	0.400	IIIc	13.7(7)	2.03(2)	7.5(4)	1.17(2)	—	0.000
	0.425	IIIc	13.0(6)	1.75(2)	8.1(5)	1.40(2)	—	0.000
	0.450	IIIc	14.2(9)	1.52(3)	7.7(4)	1.58(3)	—	0.000
	0.500	IVc	13.0(8)	1.19(2)	9.0(4)	1.81(2)	—	0.000
Cs	0.500	IVa	—	0.000	9.4(2)	3.000	—	0.000

3.3. $(PbF_2)_{1-x}$–$(CsF)_x$

The binary phase diagram for the $(PbF_2)_{1-x}$–$(CsF)_x$ system indicates the presence of a single line phase at $x = 0.500$ [32]. This observation is supported in this work, with deviations from

$x = 0.500$ composition producing samples with an excess of either PbF_2 or CsF as a second phase. As such, there is no solid solution of the type observed in the $(PbF_2)_{1-x}$–$(KF)_x$ and $(PbF_2)_{1-x}$–$(RbF)_x$ systems.

The temperature dependence of the ionic conductivity σ for the $(PbF_2)_{1-x}$–$(CsF)_x$ sample with $x = 0.500$ is illustrated in figure 9. The material has a moderately high value of σ at ambient temperature but its value does not increase rapidly with temperature and, in particular, there is no transition to a superionic state observed up to $T \sim 700$ K. The neutron diffraction data collected with the $x = 0.500$ sample at ambient temperature indicated that the material was primitive cubic with $a = 4.8001(2)$ Å, in accord with previous reports [32]. Data collected at $T = 690(2)$ K were fitted in the same manner as described in the previous two subsections, with the values of χ^2 listed in table 2. The fitting procedure clearly indicated that the structure of the material is described by model IVa, with an ordered arrangement of Pb^{2+} and Cs^+ and the F^- arranged to completely fill the three F_{oct1} positions at 0, 0, 1/2, etc. Subsequent refinements of data collected at ambient temperature and at $T = 770$ K, 820 K and 870 K illustrated that the structure remains unchanged and there is no evidence of a superionic transition up to $T \sim 870$ K. The melting point was confirmed to be at $T \sim 890$ K, contrary to the previous report which suggested a solid–solid phase transition at this temperature [32]. In support of this finding, an x-ray diffraction investigation at high temperature showed such a structural transition only in samples that had been exposed to moisture.

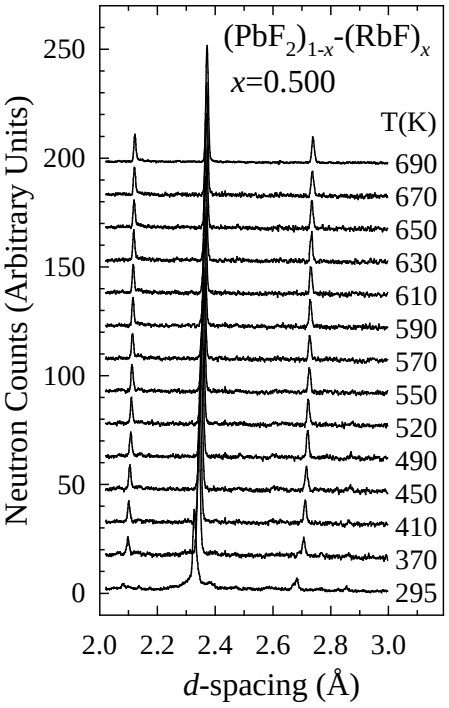

Figure 8. The evolution of the neutron diffraction pattern of the $(PbF_2)_{1-x}$–$(RbF)_x$ sample with $x = 0.500$ with temperature. The data collected at 295 K appear to be similar to those collected for the high-temperature superionic phase, though with broader peaks and the presence of additional weaker reflections.

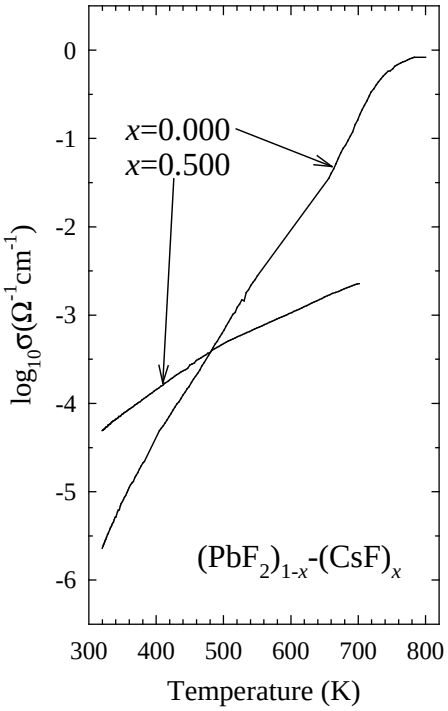

Figure 9. Variation of the ionic conductivity $\log_{10}\sigma$ with temperature for the $(PbF_2)_{1-x}$–$(CsF)_x$ sample with $x = 0.500$. For comparison, the behaviour of the fluorite-structured pure β-PbF_2 (i.e. $x = 0.000$) material is also shown.

4. Discussion

4.1. Overview

The combined use of impedance spectroscopy and neutron diffraction techniques has established the stability fields of the cubic ($Im\bar{3}m$ or $Pm\bar{3}m$) phases in the three binary systems $(PbF_2)_{1-x}$–$(MF)_x$. For $M = K^+$, the transition to the cubic phase occurs at $T \sim 520$–590 K and the high-temperature modification is superionic. This phase possesses $Im\bar{3}m$ symmetry and is stable as a single phase from $x = 0.333$ to $x \sim 0.68$, at which composition the material becomes a two-phase mixture on further increase of x. For $M = Rb^+$, the transition temperature is somewhat higher at $T \sim 570$–620 K; the high-temperature phase is superionic with space group $Pm\bar{3}m$ and is stable from $x = 0.333$ to $x = 0.500$. At compositions outside this range the cubic phase coexists with a proportion of PbF_2 ($x < 0.333$) or RbF ($x > 0.500$). Lastly, for $M = Cs^+$ there is only a single line phase of composition $x = 0.500$ which has a modest value of ionic conductivity σ and adopts an ordered primitive cubic structure up to the highest temperature measured ($T = 870$ K). Some modifications to the more complex binary phase diagrams reported for $(PbF_2)_{1-x}$–$(KF)_x$, $(PbF_2)_{1-x}$–$(RbF)_x$ and $(PbF_2)_{1-x}$–$(CsF)_x$ [32] are required to reconcile our findings with the previous work. However, this process is made difficult by the lack of agreement among the different authors concerning the ordered phases present [31–33].

Within the superionic phases of the $(PbF_2)_{1-x}$–$(KF)_x$ and $(PbF_2)_{1-x}$–$(RbF)_x$ systems the ionic conductivity does not vary significantly with temperature (see figures 1 and 4). This feature is in accord with Rietveld refinements of the neutron diffraction data collected as a function of temperature for the $x = 0.333$ ($M = K^+$), $x = 0.333$ ($M = Rb^+$) and $x = 0.500$ ($M = Rb^+$) samples. The diffraction data for the latter two cases are illustrated in figures 6 and 8, respectively. The results show no significant changes in the occupancies of the tetrahedral and octahedral sites with temperature. However, it is clear that the dopant composition and the dopant species have a more dominant influence on the nature of the thermally induced disorder than temperature and we therefore discuss these in more detail in the following subsections.

4.2. $(PbF_2)_{1-x}$–$(KF)_x$

With reference to figure 3(a), in the cation-disordered ($Im\bar{3}m$) arrangement each F_{tet} site has four nearest-neighbour (n.n.) F_{tet} sites at a distance $\sqrt{2}a/4$ and two more next-nearest-neighbour (n.n.n.) F_{tet} sites at a distance $a/2$. If we consider the ionic radius of F^- ($r_{F^-} = 1.33$ Å [34]) and the measured lattice parameter ($a = 4.6755$ Å at $T = 675$ K), it follows that the presence of an anion at one of the F_{tet} sites precludes the simultaneous occupancy of either the n.n. or n.n.n. sites because their proximity is less than $2r_{F^-}$. As a result, the maximum number of F^- that can be accommodated within the unit cell on the F_{tet} sites is three. However, the $x = 0.333$ sample has $m_{F^-} = 2(2-x) = 3.333$ and the 'excess' anions must be accommodated at octahedral sites. These steric constraints are a direct consequence of the relatively large size of the F^- (compared to Pb^{2+}, which has $r_{Pb^{2+}} = 1.19$ Å [34]). In the b.c.c.-structured Ag^+ and Cu^+ halide and chalcogenide superionics it is the smaller cation species which is mobile, such that the occupancy of a tetrahedral site does not allow the n.n. sites to be filled but does allow the n.n.n. ones to be occupied. It is then possible to accommodate six cations at tetrahedral sites within the unit cell and occupancy of octahedral positions is not required in, for example, α-AgI ($m_{Ag^+} = 2$) [24, 25] or γ-Ag_2Te ($m_{Ag^+} = 4$) [35, 36].

In the case of $(PbF_2)_{1-x}$–$(KF)_x$, this discussion provides a plausible explanation for the variation of the high-temperature ionic conductivity σ, the unit-cell constant a and the anion occupancies m_{tet} and m_{oct} versus K^+ content x (shown in figure 2). At the highest concentration

for which least-squares refinements of the diffraction data were performed ($x = 0.600$), it is clear that the proportion of anions residing on F_{tet} sites is lower than at $x = 0.333$. On decreasing x from 0.600 to 0.500, the (relatively low) occupancy of the F_{oct} sites remains essentially constant and the extra 0.2 anions per unit cell are predominantly accommodated at the available F_{tet} sites. Since the occupancy of the F_{tet} sites is less than three, this filling of 'empty' sites is not expected to expand the lattice significantly. Instead, the lattice constant a falls over the range from $x = 0.700$ to $x = 0.500$ due to the decreasing concentration of the larger K^+ cations. At $x = 0.500$, the occupancy of the F_{tet} sites saturates at $m_{tet} \sim 2.5$. This value is somewhat lower than the limiting value of three predicted by our simple argument above but full occupancy of the F_{tet} sites could not be reconciled with the observed superionic behaviour, because such a configuration would not allow hopping of anions to neighbouring (empty) F_{tet} sites.

On further decrease in K^+ content below $x = 0.500$, the additional anions are accommodated at octahedral sites. These sites are 'unfavoured' in that the octahedral coordination is somewhat distorted with two anion–cation distances of $a/2$ and four of $a/\sqrt{2}$. The former is less than both the two sums of the ionic radii $r_{F^-} + r_{Pb^{2+}}$ and $r_{F^-} + r_{K^+}$. As a result, a tendency towards expansion of the lattice is expected (as observed), even if local short-range ordering of the two cation species places two (smaller) Pb^{2+} at the two shorter distances. Finally, it is interesting to note that the trend in the ionic conductivity follows that of the F_{tet} occupancy, suggesting that these sites play a central role in the rapid ionic diffusion. In contrast, the presence of anions at the octahedral sites does not appear to be linked to high ionic conductivity, possibly because their occupancy requires a degree of reorganization of both the surrounding anion and cation sublattices (for a discussion of possible defect models, see [23]).

4.3. $(PbF_2)_{1-x}$–$(RbF)_x$

The reduction in symmetry from $Im\bar{3}m$ to $Pm\bar{3}m$ is associated with the onset of cation ordering. It is clear from the results presented in table 3 that the $(PbF_2)_{1-x}$–$(RbF)_x$ compounds locate the dominant Pb^{2+} species at the sites at 0, 0, 0 with the 1/2, 1/2, 1/2 positions occupied by the entire Rb^+ dopant content plus the remaining Pb^{2+}. In comparison with the $(PbF_2)_{1-x}$–$(KF)_x$ case, this segregation of the two chemical species is presumably a consequence of their greater size difference. The exception is the lowest-doping case ($x = 0.333$) for which there is a small, but significant, quantity of Rb^+ at the 0, 0, 0 positions. As such, this composition is tending towards the fully random occupancy of the two cation sites observed in the KF-doped system. This similarity is borne out in the distribution of the anions, which are predominantly located at F_{tet} sites but with the remainder distributed unequally over the F_{oct1} and F_{oct2} positions. Indeed, the relationship between the ordering of the two cation species and the occupancy of the F_{oct2} position is straightforward. If the Rb^+ and Pb^{2+} segregate onto the 0, 0, 0 and 1/2, 1/2, 1/2 sites, respectively (as far as allowed by the chemical composition if $x \neq 0.500$), then the F_{oct1} sites have two of the smaller Pb^{2+} cations as nearest neighbours and four of the larger Rb^+ as next-nearest neighbours. These F_{oct1} sites are clearly energetically favoured over the F_{oct2} ones which have the larger cations at the shorter contact distance (see figure 3(b)). This intuitive suggestion is supported by the fits to the neutron diffraction data which show no evidence for the occupancy of the F_{oct2} sites at $x > 0.333$. Instead, the tendency towards complete segregation of Pb^{2+} and Rb^+ as x increases is accompanied by a change in the preferred anion occupancy towards the octahedral rather than the tetrahedral sites. This can be interpreted as a tendency towards a cubic perovskite-type arrangement. In common with the K^+-doped case, the ionic conductivity behaviour again mirrors the occupancy of the F_{tet} sites. However, the

occupancy of the F_{oct1} sites (which is, of course, a consequence of the cation segregation) is less likely to influence the lattice parameter significantly and a is then observed to increase simply because the concentration of the larger Rb^+ ions increases.

4.4. $(PbF_2)_{1-x}$–$(CsF)_x$

The trend towards ordered cubic perovskite-like structure observed in the $(PbF_2)_{1-x}$–$(RbF)_x$ system as x increases is achieved in the case of $(PbF_2)_{1-x}$–$(CsF)_x$ with $x = 0.500$. This composition can, therefore, be written as $CsPbF_3$ to explicitly illustrate its relationship to an ideal perovskite-structured compound of stoichiometry ABX_3. There is no superionic transition in this material up to $T = 870(5)$ K, with the neutron diffraction data providing no evidence for even limited disorder of either the anion or the cation sublattice.

With reference to figure 3(b), it is clear that the cation environment surrounding the F_{tet} site is irregular, comprising two M^+ and two Pb^{2+}. The ionic radius of Cs^+ ($r_{Cs^+} = 1.67$ Å [34]) is significantly larger than that of Rb^+ and K^+ and the size difference between M^+ and Pb^{2+} is greatest in the case of $CsPbF_3$. This has the tendency to displace the centre of the tetrahedral hole away from its ideal $1/4, 0, 1/2$ position towards the occupied F_{oct1} site at $0, 0, 1/2$. As a consequence, the F_{tet} site can no longer be considered to be an isolated vacant site and the absence of significant F^- occupancy at these positions determined by the fits to the neutron diffraction data can be readily understood.

The implications of these findings for the question of possible superionic behaviour within perovskite-structured compounds are discussed in the following subsection.

4.5. Perovskite-structured superionics

In the case of the binary compounds such as AgI, CuI, CuBr and Ag_2Te, it is generally accepted that superionic behaviour is favoured in those phases which have a b.c.c. sublattice formed by the immobile (anion) species, rather than an f.c.c. one [2]. The justification lies in the preferential occupancy of the mobile Ag^+ and Cu^+ at tetrahedral sites (rather than octahedral ones) and the presence of six such sites per anion in the b.c.c. case and only two in the f.c.c. case. On these simple grounds, ternary ABX_3 compounds which possess the perovskite crystal structure should be promising candidates for exhibiting high-temperature superionic behaviour because the A and B cations form a b.c.c. array. There are four tetrahedral sites available per (mobile) anion, an important requirement in light of the evidence provided by figures 2 and 5 that the ionic conductivity σ is highest for those compositions which have the greatest occupancy of the F_{tet} sites.

However, the ordering of the two cation species over the $0, 0, 0$ and $1/2, 1/2, 1/2$ positions and the resultant change in symmetry from $Im\bar{3}m$ to $Pm\bar{3}m$ has important consequences. As discussed in previous subsections, three of the six F_{oct} sites (labelled F_{oct2} in our notation) become energetically unfavoured and the mean position of the F_{tet} sites is displaced towards the 'favoured' F_{oct1} positions. The resultant structural picture tends towards essentially isolated F_{oct1} sites and implies that an ordered cation arrangement is unlikely to promote superionic behaviour. This, in turn, suggests that high anion mobility only occurs if the two cation species are of similar size. However, the latter criterion is at odds with the stability requirements of the cubic perovskite structure. As discussed by Hyde and Andersson [37], the perovskite structure is 'overdetermined' in that there is only one variable structural parameter, the cubic lattice parameter a. The structure must, therefore, simultaneously meet the two bond-length criteria $r_A + r_X = a/\sqrt{2}$ and $r_B + r_X = a/2$, which imply that r_A is significantly larger than r_B. This argument is the basis of the Goldschmidt tolerance factor $S = (r_A + r_X)/\sqrt{2}(r_B + r_X)$ which

predicts that the compound will adopt a cubic perovskite structure if $1.05 > S > 0.95$ and a distorted version formed by cooperative buckling of the corner-sharing BX_6 octahedra if $0.95 > S > 0.75$.

In summary, the requirements of superionic behaviour and the stability of the cation-ordered perovskite structure appear to be conflicting. Clearly, this discussion is somewhat speculative and we must be wary of generalization solely on the basis of the three $(PbF_2)_{1-x}$–$(MF)_x$ systems discussed in this paper, particularly in view of the uncertain nature of the experimental evidence for other compounds (see section 1). However, it is interesting to note that of the four perovskite-related $KB^{2+}F_3$ compounds, superionic behaviour has been reported for those with the lowest cation radius ratio ($KCaF_3$ with $r_{K^+}/r_{Ca^{2+}} = 1.65$ and $KZnF_3$ with $r_{K^+}/r_{Zn^{2+}} = 2.21$ [34]) and not for those with the highest ($KMgF_3$ with $r_{K^+}/r_{Mg^{2+}} = 2.28$ and $KMnF_3$ with $r_{K^+}/r_{Mn^{2+}} = 2.45$ [34]). For comparison, the superionic phases $KPbF_3$ and $RbPbF_3$ have corresponding values of 1.37 and 1.45, respectively, whilst $CsPbF_3$ has a higher value of 1.57.

5. Conclusions

The experimental work presented in this paper demonstrates the remarkable nature of the compound PbF_2 and its important role in the study of the superionic state. In its pure state it is the 'best' fluorite-structured superionic. Dopings with relatively low concentrations of aliovalent cations (e.g. K^+ and Y^{3+}) significantly enhance the ionic conductivity at room temperature [5–7]. In the case of the monovalent cations, further doping forms the cubic superionic phases described in this work. At the limit of high dopant concentration x in the $(PbF_2)_{1-x}$–$(KF)_x$ system, the high-temperature anion superionic phase is essentially an anti-type to the cation-mobile α-AgI and γ-Ag_2Te-type phases, with the majority of the mobile ions undergoing rapid hops between the tetrahedral voids. In the case of $CsPbF_3$, no superionic behaviour is observed and the compound adopts a fully ordered perovskite structure up to the melting point. As such, the $(PbF_2)_{1-x}$–$(MF)_x$ compounds with $M = K^+$, Rb^+ and Cs^+ clearly illustrate the structural link between the archetypal b.c.c.-structured superionic phases and the ternary compounds with the perovskite structure. It is hoped that this experimental work will motivate further theoretical studies of systems of this type, including molecular dynamics simulations, to probe the diffusion process at the ionic level.

Acknowledgments

We are extremely grateful to J Dreyer, J Bones, R Humphreys and N J G Gardner for their assistance with the development of the complex-impedance-spectroscopy apparatus. One of the authors (PB) wishes to thank the Swedish Foundation for International Cooperation in Research and Higher Education for financial support.

References

[1] Chandra S 1981 *Superionic Solids. Principles and Applications* (Amsterdam: North-Holland)
[2] Boyce J B and Huberman B A 1979 *Phys. Rep.* **51** 189
[3] Hutchings M T, Clausen K, Dickens M H, Hayes W, Kjems J K, Schnabel P G and Smith C 1984 *J. Phys. C: Solid State Phys.* **17** 3903
[4] Schröter W and Nolting J 1980 *J. Physique Coll.* **41** 20
[5] Liang C C and Joshi A V 1975 *J. Electrochem. Soc.: Electrochem. Sci. Technol.* **122** 466
[6] Ito Y, Mukoyama T, Kanamaru F and Yoshikado S 1994 *Solid State Ion.* **73** 283
[7] Reau J M, Federov P P, Rabardel L, Mater S F and Hagenmuller P 1983 *Mater. Res. Bull.* **18** 1235

[8] Chadwick A V, Strange J H, Ranieri G A and Terenzi M 1983 *Solid State Ion.* **9+10** 555
[9] Andersen N H, Kjems J K and Hayes W 1985 *Solid State Ion.* **17** 143
[10] Watson G W, Parker S C and Wall A 1992 *J. Phys.: Condens. Matter* **4** 2097
[11] Boyett R E, Ford M G and Cox P A 1995 *Solid State Ion.* **81** 61
[12] Watson G W, Wall A and Parker S C 1995 *Phys. Earth Planet. Inter.* **89** 137
[13] Poirier J P, Peyronneau J, Gesland J Y and Brebec G 1983 *Phys. Earth Planet. Inter.* **32** 273
[14] O'Keeffe M and Bovin J-O 1979 *Science* **206** 599
[15] Zhou L X, Hardy J R and Cao H Z 1997 *Geophys. Res. Lett.* **24** 747
[16] Street J N, Wood I G, Knight K S and Price G D 1997 *J. Phys.: Condens. Matter* **9** L647
[17] Ridou C, Rousseau M, Pernot B and Bouillot J 1986 *J. Phys. C: Solid State Phys.* **19** 4847
[18] Cahn R W 1984 *Nature* **308** 493
[19] Matsui M and Price G D 1991 *Nature* **351** 735
[20] Karato S I and Li P 1992 *Science* **255** 1238
[21] Gautason B and Muehlenbachs K 1993 *Science* **260** 518
[22] Liu L-G and Bassett W A 1986 *Elements, Oxides, Silicates. High Pressure Phases with Implications for the Earth's Interior* (Oxford: Oxford University Press)
[23] Hull S, Berastegui P, Eriksson S G and Gardner N J G 1998 *J. Phys.: Condens. Matter* **10** 8429
[24] Wright A F and Fender B E F 1977 *J. Phys. C: Solid State Phys.* **10** 2261
[25] Nield V M, Keen D A, Hayes W and McGreevy R L 1993 *Solid State Ion.* **66** 247
[26] Gardner N J G, Hull S, Keen D A and Berastegui P 1998 *Rutherford Appleton Laboratory Report* RAL-TR-1998-032
[27] Hull S, Smith R I, David W I F, Hannon A C, Mayers J and Cywinski R 1992 *Physica* B **180+181** 1000
[28] David W I F, Ibberson R M and Matthewman J C 1992 *Rutherford Appleton Laboratory Report* RAL-92-032
[29] Brown P J and Matthewman J C 1987 *Rutherford Appleton Laboratory Report* RAL-87-010
[30] *International Tables for Crystallography* 1995 vol C, ed A J C Wilson (Dordrecht: Kluwer)
[31] Pistorius C W F T and van Rensburg J E J 1971 *Z. Anorg. Allg. Chem.* **383** 204
[32] Schmitz-Dumont O and Bergerhoff G 1956 *Z. Anorg. Allg. Chem.* **283** 314
[33] Botalov A I and Korenov Y M 1996 *Zh. Neorg. Khim.* **41** 962
[34] Shannon R D and Prewitt C T 1969 *Acta Crystallogr.* B **25** 925
[35] Schneider J and Schulz H 1993 *Z. Kristall.* **203** 1
[36] Keen D A and Hull S 1998 *J. Phys.: Condens. Matter* **10** 8217
[37] Hyde B G and Andersson S 1989 *Inorganic Crystal Structures* (New York: Wiley–Interscience)